

STARFormer: A Novel Spatio-Temporal Aggregation Reorganization Transformer of fMRI for Brain Disorder Diagnosis

Wenhao Dong[✉], Yueyang Li[✉], Weiming Zeng[✉], *Senior Member, IEEE*, Lei Chen[✉],
Hongjie Yan[✉], Wai Ting Siok[✉], and Nizhuan Wang[✉]

Abstract—Many existing methods that use functional magnetic resonance imaging (fMRI) classify brain disorders, such as autism spectrum disorder (ASD) and attention deficit hyperactivity disorder (ADHD), often overlook the integration of spatial and temporal dependencies of the blood oxygen level-dependent (BOLD) signals, which may lead to inaccurate or imprecise classification results. To solve this problem, we propose a Spatio-Temporal Aggregation Reorganization Transformer (STARFormer) that effectively captures both spatial and temporal features of BOLD signals by incorporating three key modules. The region of interest (ROI) spatial structure analysis module uses eigenvector centrality (EC) to reorganize brain regions based on effective connectivity, highlighting critical spatial relationships relevant to the brain disorder. The temporal feature reorganization module systematically segments the time series into equal-dimensional window tokens and captures multiscale features through variable window and cross-window attention. The spatio-temporal feature fusion module employs a parallel transformer architecture with dedicated temporal and spatial branches to extract integrated features. The proposed STARFormer has been rigorously evaluated on two publicly available datasets for the classification of ASD and ADHD. The experimental results confirm that the STARFormer achieves state-of-the-art performance across multiple evaluation metrics, providing a more accurate and reliable tool for the diagnosis of brain disorders and biomedical research. The codes will be available at: <https://github.com/NZWANG/STARFormer>.

Index Terms—Brain disorder diagnosis, fMRI, eigenvector centrality, spatio-temporal information integration, transformer.

This work was supported by the National Natural Science Foundation of China [grant number 31870979], the Hong Kong Polytechnic University Faculty Reserve Fund (Project ID: P0053738), and the Hong Kong Polytechnic University Start-up Fund (Project ID: P0053210). ((Wenhao Dong and Yueyang Li are co-first authors) (Corresponding author: Weiming Zeng and Nizhuan Wang)).

Wenhao Dong, Yueyang Li, Weiming Zeng and Lei Chen are with the Laboratory of Digital Image and Intelligent Computation, College of Information Engineering, Shanghai Maritime University, Shanghai 201306, China (email: jsxdwh@163.com, lyy20010615@163.com, zengwm86@163.com, chen.sanshi@163.com).

Hongjie Yan is with the Department of Neurology, Affiliated Lianyungang Hospital of Xuzhou Medical University, Lianyungang 222002, China (email: yanhjns@gmail.com).

Wai Ting Siok and Nizhuan Wang are with the Department of Chinese and Bilingual Studies, The Hong Kong Polytechnic University, Hong Kong SAR, China (e-mail: wai-ting.siok@polyu.edu.hk, wang-nizhuan1120@gmail.com).

I. INTRODUCTION

THE human brain function can be characterized by intricate functional networks where multiple brain regions cooperate to facilitate cognitive processes and mental states [1]. Disruptions of these networks can manifest as various neurodevelopmental conditions, such as autism spectrum disorder (ASD) [2] and attention deficit hyperactivity disorder (ADHD) [3]. However, the underlying mechanisms of these disruptions are not yet fully understood [4]–[6]. Resting-state functional magnetic resonance imaging (rs-fMRI) has emerged as a powerful, noninvasive technique for investigating these functional networks by measuring blood oxygen-level-dependent (BOLD) signals with relatively high spatial and temporal resolution [7]. In particular, functional connectivity (FC), which reflects the temporal correlations of BOLD signals between regions of interest (ROI), provides crucial insights into brain organization and cognitive functions [8], [9].

Traditional diagnostic approaches, which primarily rely on symptomatic observations and clinical expertise, are inadequate for detecting intricate patterns across the entire brain. This limitation highlights the need for more advanced analytical methods. Initially, traditional machine learning techniques were used to analyze multivariate brain responses from rs-fMRI data for diagnosing neurodevelopmental disorders [10]. The field then progressed with the advent of deep learning [11] and, more recently, the groundbreaking introduction of transformer models [12]. Transformers have significantly improved the modeling of complex patterns in high-dimensional data through self-attention mechanisms, offering better scalability and more efficient capture of global network information than conventional approaches [13], [14]. However, traditional transformer models often struggle to capture both the intricate spatial and temporal features within fMRI data simultaneously. The standard self-attention mechanism in transformer encoders tends to focus on identifying parts of the time series with similar patterns across the entire sequence, especially those with matching peaks. This approach may overlook patterns that are similar in the short to medium term, as they occur closely in time. In fMRI data analysis, recognizing these short-to-medium-term patterns is crucial because significant changes in BOLD signals may only occur within shorter time windows, rather than being consistent throughout the entire duration

[15].

To address these limitations, we propose a novel spatio-temporal aggregation reorganization transformer (STARFormer) that effectively captures both spatial and temporal information of brain functional networks through a designed dual-branch architecture. This approach uses effective connectivity to provide spatial information for the time series of BOLD signals. Unlike methods that rely solely on FC, this approach preserves temporal dynamics while incorporating spatio-temporal information. Our methodology introduces three key innovations:

1) **ROI Spatial Structure Analysis Module:** This module employs eigenvector centrality (EC) to reorganize brain regions based on their functional importance within seven established brain networks, ensuring the preservation and enhancement of crucial spatial relationships. This reorganization significantly improves the model’s ability to identify disorder-related spatial patterns.

2) **Temporal Feature Reorganization Module:** This module integrates multiscale local features with global representations through a unique variable window strategy, enabling the model to capture fine-grained temporal patterns at different scales while maintaining computational efficiency. The implementation of cross-window attention enhances the model’s capacity to capture both short-term and long-term temporal dependencies in time series.

3) **The Spatio-Temporal Feature Fusion Module:** This module comprises temporal and spatial branches that simultaneously extract multiscale temporal dependencies and spatial representations. The temporal branch incorporates the temporal feature reorganization module to learn local and global temporal features, while the spatial branch uses the reorganized ROI structure to capture disorder-specific patterns.

These innovations collectively make STARFormer a powerful tool that significantly enhances the accuracy and efficiency of diagnosing brain disorders by capturing critical spatio-temporal features. Overall, the contributions of our work are summarized as follows.

- A transformer architecture is proposed to enhance brain-disorder diagnosis by integrating disorder-specific ROI spatial information, thereby improving the precision and efficiency of fMRI analysis.
- A novel variable window-based temporal feature reorganization module is included, allowing STARFormer to capture both local and global features by adjusting window size.
- A spatio-temporal feature fusion module is developed to fully explore deep spatio-temporal features, enabling comprehensive feature representation.

II. RELATED WORK

A. Centrality Nodes Identification in Brain Disorders

Identifying critical brain nodes is crucial for understanding disorder-specific functional disruptions, as neurological disorders significantly differ in regional connectivity patterns [16]. For example, individuals with mild cognitive impairment exhibit altered effective connectivity in memory-related areas

such as the hippocampus and amygdala [17], while individuals with ASD display distinctive alterations in regions associated with social cognition, such as the default mode network [18].

Measures of node centrality have been effectively applied in diagnosing brain disorders to uncover differential patterns. For example, Saha [19] used EC to assess group differences in the centrality of brain regions, distinguishing between typically developing children and those with ASD. Similarly, Grobelyny et al. [20] utilized betweenness centrality (BC) to construct diagnostic models for pediatric epilepsy, revealing that nodes with high BC during seizure onset could represent centers in self-regulating networks that help terminate seizures. Liao et al. [21] found that changes in degree centrality (DC) in Parkinson’s disease were frequency-related and frequency-specific. However, due to computational complexity, BC, DC and other centrality measurement methods are less suitable for analyzing full-brain networks that involve a large number of voxels [19]. Hence, this study focuses on EC to identify differential connectivity patterns, highlighting the importance of key nodes in distinguishing pathological alterations.

B. Features of fMRI for Brain Disorders Identification

The extraction of FC features is a key focus in many neuroimaging studies. A typical approach for identifying brain disorders involves extracting FC, which represents the temporal correlation matrix of BOLD signals from ROI, followed by the use of classifiers such as SVM and logistic regression to reduce dimensionality [10]. A study by [22] proposed a novel architecture called local sequential feature coupling global representation learning (LCGNet), which uses convolution operations and self-attention mechanisms to enhance representation learning in fully convolutional networks for automatic brain disorder classification. However, FC is limited to capturing linear relationships and lacks causal or directional insights. The effective connectivity approach has emerged as a promising tool that describes brain activity by incorporating causal interactions between brain regions [23]. The study by Dai et al. [24] indicated that patients with major depressive disorder (MDD) exhibit significantly altered effective connectivity networks in various brain networks during the resting state, which may serve as potential biomarkers. Unlike FC, which focuses solely on statistical correlations, effective connectivity elucidates the directional influence between regions, providing a deeper understanding of the connections within the brain [25].

Although deep learning methods based on FC have been widely used for diagnosing brain disorders, some studies reveal that these methods can overlook the temporal nature of fMRI data, thereby losing vital information on temporal dynamics [26]. Recent advances in time-domain-based deep learning methods have shown great promise in diagnosing brain disorders. For instance, long short-term memory (LSTM) networks have been used to classify individuals with ASD and typical controls from multi-site fMRI time series [27], while a transformer model with a fusion window has further advanced fMRI time series analysis [28].

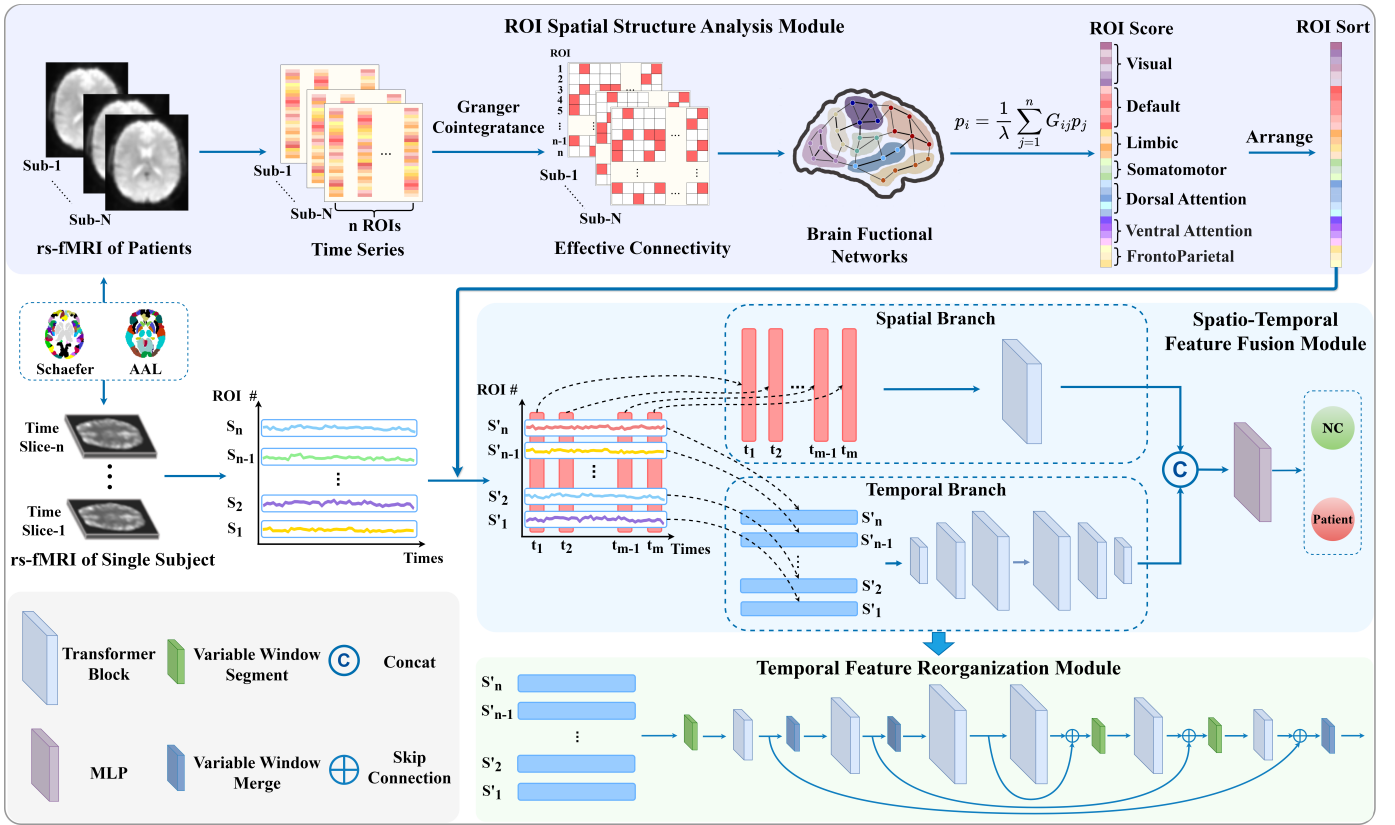


Fig. 1. Architecture of STARFormer in fMRI data for brain disorder diagnosis.

C. Spatio-Temporal Information Integration for Brain Disorders Identification

For modeling fMRI features, most deep learning models do not fully exploit the spatial and temporal dependencies of fMRI signals, limiting the precise analysis of brain activity. The gradient-weighted Markov random field (gwmRF) model mentioned in [29] enables spatially-ordered brain region extraction. This study demonstrated that spatial disorganization decreases model performance, emphasizing the need to preserve spatial information in rs-fMRI. Recent studies increasingly emphasize the importance of spatio-temporal information integration. For example, the use of 3D-CNNs can extract spatial features from fMRI data for diagnosing ASD and ADHD [30], [31]. Liu et al. [32] proposed STCAL, a spatio-temporal cooperative attention learning model that employs a guided cooperative attention module to simultaneously capture spatio-temporal correlations and learn fine-grained attention representations from time series fMRI data. Zhang et al. [33] used independent component analysis (ICA) to aggregate spatio-temporal information from fMRI, improving the performance of depression diagnosis.

Transformer models have also made significant advances in integrating spatio-temporal features, showcasing their potential to capture complex dependencies within fMRI data. In [26], a novel transformer-based framework, the ST-Transformer, was introduced, featuring a linear spatio-temporal multihead attention unit to extract spatio-temporal features from fMRI data through spatial self-attention. Similarly, a spatio-temporal

graph transformer network was proposed in [34], incorporating a spatial transformer-based graph message-passing mechanism to capture inter-regional relationships and using FC as edge features.

III. METHOD

An overview of STARFormer combining the spatial and temporal information is illustrated in Fig. 1. It consists of the ROI spatial structure analysis module, the temporal feature reorganization module and the spatio-temporal feature fusion module.

A. ROI Spatial Structure Analysis Module

The spatial information of the brain is provided by the effective connectivity matrix \mathbf{G} of N patients. We use Granger causality (GC) to calculate effective connectivity between different brain regions, as it can reveal whether the time series of a brain region predict the time series of another [35]. Suppose the chosen atlas divides the brain into n ROIs, each with a time series $s_i(t)$ of length m . We first establish an autoregressive model, where the time series of each ROI i can be predicted using its own values from the past h time points:

$$s_i(t) = \sum_{k=1}^h a_{ik}s_i(t-k) + \varepsilon_i(t), \quad (1)$$

where a_{ik} is the regression coefficient and $\varepsilon_i(t)$ is the prediction error or residual.

Then, a bivariate GC model is constructed to test for Granger causal effects between ROI:

$$s_j(t) = \sum_{k=1}^h a_{jk}s_j(t-k) + \sum_{k=1}^h b_{ik}s_i(t-k) + \varepsilon'_j(t), \quad (2)$$

where b_{ik} is the coefficient of influence of node i on node j . Subsequently, the residual variances of both models are computed and an F-test is used to evaluate whether the models exhibit a statistically significant difference. A significant F-value indicates that the time series of ROI i Granger-causes the time series of ROI j . For each pair of ROI (i, j) , the results of the GC test are indicated as G'_{ij} , where $G'_{ij} = 1$ indicates a GC relationship from ROI i to ROI j , while $G'_{ij} = 0$ indicates the absence of such a relationship. Finally, a valid connection matrix \mathbf{G} for $n \times n$ can be constructed as

$$\mathbf{G} = \begin{pmatrix} 0 & G_{12} & \cdots & G_{1n} \\ G_{21} & 0 & \cdots & G_{2n} \\ \vdots & \vdots & \ddots & \vdots \\ G_{n1} & G_{n2} & \cdots & 0 \end{pmatrix}. \quad (3)$$

The ROIs and the connectivity metrics of the effective connectivity matrix \mathbf{G} define the nodes and edges of the graph, respectively. Serving as the adjacency matrix of the network, \mathbf{G} facilitates the assessment of node centrality through its eigenvectors. EC quantifies the importance of the nodes within the network by considering not only the number of connections each node possesses, but also the importance of the nodes to which it is connected. The EC score p_i for each ROI i measures its connection strength to other influential ROIs in the network and can be expressed as

$$p_i = \frac{1}{\lambda} \sum_{j=1}^n G_{ij}p_j, \quad (4)$$

where λ is the largest eigenvalue of \mathbf{G} , and G_{ij} represents the connectivity measure from ROI i to ROI j .

The EC problem can be expressed in matrix form as

$$\mathbf{G}\mathbf{P} = \lambda\mathbf{P}, \quad (5)$$

where $\mathbf{P} = [p_1, p_2, \dots, p_n]^T$ represents the EC vector, with λ denoting its corresponding eigenvalue. The calculation requires determining the principal eigenvector \mathbf{P} of the adjacency matrix \mathbf{G} in conjunction with its dominant eigenvalue λ . Subsequently, the EC of any given ROI i is precisely captured by the component p_i within this principal eigenvector associated with the maximal eigenvalue λ . To guarantee uniqueness and stability, p_i is normalized such that

$$p_i = \frac{p_i}{\sum_{i=1}^n p_i}, \quad (6)$$

thereby normalizing the centrality values.

Following the computation of the EC vector for ROIs of each patient, the average EC vector $\bar{\mathbf{P}}$ for all patients was determined by

$$\bar{p}_i = \frac{1}{N} \sum_{i=1}^N p_i, \quad (7)$$

$$\bar{\mathbf{P}} = [\bar{p}_1, \bar{p}_2, \dots, \bar{p}_n]^T.$$

We consider using the obtained EC score \bar{p}_i of ROI to rearrange the spatial information. To reduce noise and errors caused by unrelated regional arrangements, ROIs are grouped according to the seven functional networks of the brain (visual network, somatomotor network, default network, limbic network, dorsal attention network, ventral attention and frontoparietal network) [36]. This functional network-based partition reflects the modular and distributed nature of brain function, with different functional networks responsible for processing different types of information and tasks. The ROIs within each group are then arranged by \bar{p}_i in descending order:

$$\begin{aligned} \text{Network}_{k_i} &= \{ROI_1, ROI_2, \dots, ROI_r\}, \\ \text{Network}'_{k_i} &= \text{Arranging}(\text{Network}_{k_i}), \end{aligned} \quad (8)$$

where Network_{k_i} is the i -th functional network, r denotes the number of ROIs within the functional network. The final sorting result Sort is expressed as follows:

$$\text{Sort} = \{\text{Network}'_{k_1}, \text{Network}'_{k_2}, \dots, \text{Network}'_{k_7}\}. \quad (9)$$

The global EC of ROIs allows for better capture of interactions or dependencies between regions. Rearranging ROIs aligns the order of the brain network with the spatial characteristics of the patients, improving the stability and consistency of its analysis. The sorting results of the ROIs are applied to the fMRI time series data for all participants $S = \{S_1(t), S_2(t), \dots, S_n(t)\}$, and

$$S' = \text{Ordering}(S, \text{Sort}), \quad (10)$$

where $S' = \{S'_1(t), S'_2(t), \dots, S'_n(t)\}$ represent the fMRI time series data after the application of ordering.

B. Spatio-Temporal Feature Fusion Module

The spatio-temporal feature fusion module employs a parallel network architecture consisting of temporal and spatial branches, which extract multi-level features from fMRI data without mutual interference. The temporal branch operates through a dual-phase mechanism of merge and segmentation, where input data undergoes segmentation into window tokens processed through variable windows, facilitating inter-window information exchange via cross-window attention mechanisms. Meanwhile, the spatial branch maintains a fundamental transformer architecture with standard self-attention mechanisms for spatial information extraction. This enables STARFormer to effectively leverage the node spatial information derived from the ROI spatial structure analysis module to uncover disorder-related latent spatial representations.

Arrayed rs-fMRI data S' are used as input to the spatio-temporal feature fusion module. S' enter the temporal branch and the spatial branch, respectively. The temporal branch treats each row $S'_i(t)$ in S' as a token, allowing the cross-window attention in the temporal branch to learn local features. When inputting into the spatial branch, the spatial branch adjusts the dimensions of S' to $m \times n$ as the new input $S^T = \{t_1, t_2, \dots, t_m\}$, treating each column t_i in S' as a token. Self-attention in the spatial branch can learn the global dependencies between brain regions. The results obtained

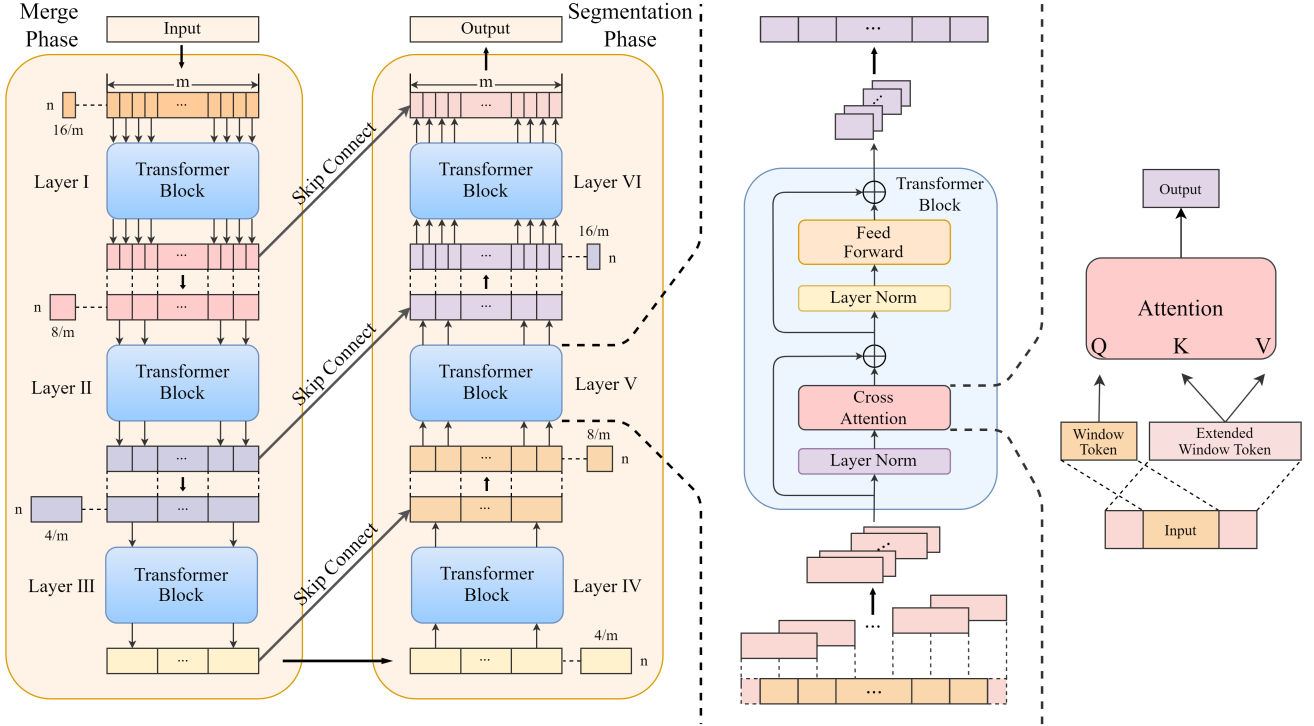


Fig. 2. Architecture of the temporal feature reorganization module in STARFormer, which employs variable window and cross-window attention to capture both local temporal patterns and global dependencies in fMRI data.

from the two branches are then integrated, and the detailed operations can be expressed as

$$F = \text{Concat}[Sp(S'), Te(S^T)^T], \quad (11)$$

where Sp refers to the processing of the spatial branch and Te refers to the processing of the temporal branch. Finally, the combined feature F was input into the multilayer perceptron (MLP) for classification.

C. Temporal Feature Reorganization Module

Exclusive reliance on global similarity metrics is hypothesized to obscure critical time-dependent local patterns, potentially diminishing ability of the model to capture intricate features within fMRI data. To enhance classification accuracy while reducing computational complexity, this work introduces a novel Temporal Feature Reorganization Module based on variable window.

1) *Window Tokens and Extended Window Tokens*: In the temporal branch, the arranged fMRI time series data S' are segmented into equally sized window tokens $\{x_1^l, x_2^l, \dots, x_g^l\}$ along the temporal dimension by the variable window, where g is the number of window tokens and l is the layer of the temporal branch. The length of each window token x is $w = m/g$. The extended window token y_i is formed by extending x_i at both the start and the end of the temporal dimension by a length of $w/2$, respectively. The length of y_i is $2w$. To ensure that the lengths of the extended window tokens are consistent, padding of length $w/2$ is added to the start of the first window token x_1 and the end of the last window token x_g to form the extended window tokens y_1 and y_g , while

the overall length of the time series extends to $m + w$. It is intended that the positions of this padding do not participate in the subsequent backpropagation process, so masks will be used to cover the padded positions during training to avoid affecting the performance of the model.

2) *Transformer Block*: The window tokens will serve as inputs to the transformer block. The transformer block comprises a layer norm (LN) layer, a cross attention layer, and a feed forward (FF) layer. The LN layer is responsible for applying layer normalization to the input data, which improves the model training process. To facilitate cross-window information interaction between window tokens, the model employs cross-window attention between window tokens instead of self-attention within window tokens. The cross attention layer receives extended window tokens of length $2w$ as input. When processing a time series composed of g window tokens, let Q represent the queries in the attention mechanism, and K and V represent the keys and values, respectively. The query, key, and value can be expressed as

$$\begin{aligned} Q &= f_q(x_1, x_2, \dots, x_g), \\ K &= f_k(y_1, y_2, \dots, y_g), \\ V &= f_v(y_1, y_2, \dots, y_g), \end{aligned} \quad (12)$$

where f_q, f_k, f_v are learnable linear projections.

Performing global self-attention requires calculating the relationships between each token and all other tokens, which undoubtedly involves high computational complexity. However, using the extended window in the attention computation allows the representation of local information to no longer be limited to its own window tokens. This facilitates the

interaction of information between window tokens and reduces computational complexity. To better capture specific positional information between window tokens, bias is incorporated into the attention computation to adjust the attention weight matrix [37], [38]:

$$\text{Attention}(Q, K, V) = \text{Softmax}\left(\frac{QK^T}{\sqrt{d}} + \mathbf{B}\right)V, \quad (13)$$

where \mathbf{B} is a learnable positional bias matrix and d is the feature dimension of the attention heads. \mathbf{B} represents the positions of the window tokens relative to all the tokens in the receptive field, including both the window tokens and the extended window tokens. The FF layer applies a nonlinear transformation to the input and utilizes Dropout to prevent model overfitting. The activation function used is GELU (Gaussian error linear unit) [39].

3) *Variable Window*: In the merge phase of the temporal branch, S' will first be segmented into 16 equal-length window tokens $\{x_1^1, x_2^1, \dots, x_{16}^1\}$ and input into the transformer block for computation. In the next layer, the computed results will be sequentially merged in pairs into 8 equal-length window tokens $\{x_1^2, x_2^2, \dots, x_8^2\}$, which will then be input into the transformer block for further computation. Afterward, the resulting outputs will be sequentially merged into 4 equal-length window tokens $\{x_1^3, x_2^3, x_3^3, x_4^3\}$ for computation in the subsequent transformer block. The merge phase is then expressed as

$$\begin{aligned} x_1^l, x_2^l, \dots, x_g^l &= \text{TransformerBlock}(x_1^l, x_2^l, \dots, x_g^l), \\ x_i^{l+1} &= (x_{2i-1}^l, x_{2i}^l), i = 1, 2, \dots, g/2. \end{aligned} \quad (14)$$

In the merge phase, the number of layers $l \in \{1, 2, 3\}$ and the number of window tokens $g \in \{16, 8, 4\}$.

After entering the segment phase, the transformer block will first take the results from the previous layer as $\{x_1^4, x_2^4, x_3^4, x_4^4\}$ and perform computations again. In the next layer, the computed results will be segmented into 8 window tokens $\{x_1^5, x_2^5, \dots, x_8^5\}$ for further computation. Finally, the 8 window tokens will be segmented into 16 window tokens $\{x_1^6, x_2^6, \dots, x_{16}^6\}$ for the final computation. Additionally, skip connections are used between window tokens of the same size in both the merge and segment phases to alleviate the issues of gradient vanishing and explosion, accelerate model convergence, and reduce the complexity of the network. The segment phase is then expressed as

$$\begin{aligned} x_1^l, x_2^l, \dots, x_g^l &= \text{TransformerBlock}(x_1^l, x_2^l, \dots, x_g^l), \\ (x_{2i-1}^{l+1}, x_{2i}^{l+1}) &= x_i^l + x_i^{l-1}, i = 1, 2, \dots, g. \end{aligned} \quad (15)$$

In the segment phase, the number of layers $l \in \{4, 5, 6\}$ and the number of window tokens $g \in \{4, 8, 16\}$.

The following Algorithm 1 shows the procedure of spatio-temporal feature fusion module.

IV. EXPERIMENTS

A. Datasets

In this study, we conducted experiments using two public fMRI datasets: ABIDE-I and ADHD-200. The ABIDE-I

Algorithm 1 Pseudocode of the spatio-temporal feature fusion module

Require: The time series data of the i -th subject $S' \in R^{n \times m}$

Ensure: The predicted probability of the i -th subject set Prob

Spatial branch

$\{t_1, t_2, \dots, t_m\} \leftarrow (S')^T = \{S(t)_1', S(t)_2', \dots, S(t)_n'\}^T$

$\{t'_1, t'_2, \dots, t'_m\} \leftarrow \text{TransformerBlock}\{t_1, t_2, \dots, t_m\}$

$S^{T'} = \{t'_1, t'_2, \dots, t'_m\}^T$

Temporal branch

$S^1 \leftarrow S'$

for $l = 1, 2, \dots, 6$ **do** # l : l -th layer of temporal branch

$X^l = \{x_1^l, x_2^l, \dots, x_g^l\} \leftarrow S^l$

$Y^l = \{y_1^l, y_2^l, \dots, y_g^l\} \leftarrow \{x_1^l, x_2^l, \dots, x_g^l\}$

$\text{Compute}(Q, K, V) \leftarrow \text{LN}(X^l), \text{LN}(Y^l), \text{LN}(Y^l)$

$\text{Attention Output} \leftarrow \text{CrossAttention}(Q, K, V)$

$\text{Residual Connections} \leftarrow X^l + \text{Attention Output}$

$\text{Norm} \leftarrow \text{LN}(\text{Residual Connections})$

$S^l \leftarrow \text{FF}(\text{Norm}) + \text{Residual Connections}$

if $l > 3$ **then**

$S^l \leftarrow S^l + S^{l-1}$

end if

end for

$F = \text{Concat}(S^l, S^{T'})$

$\text{Output logits} \leftarrow \text{LinearTransformation}(F)$

$\text{Prob} \leftarrow \text{Softmax}(\text{Output logits})$

dataset was compiled by collaboration between 17 international imaging sites, openly sharing 871 valid fMRI samples from 403 individuals with ASD and 468 typically developing controls [40]. The ADHD-200 dataset was collected from 8 international imaging sites, openly sharing 947 valid fMRI samples from 362 children and adolescents with ADHD and 585 typically developing controls [41].

The preprocessed fMRI datasets are available in C-PAC of ABIDE-I and Athena of ADHD-200 [42], [43]. Specifically, the preprocessing steps include voxel intensity normalization, motion correction, and slice timing correction. The fMRI images are then co-registered to their corresponding anatomical images and normalized to MNI152 space. Finally, the mean time series is extracted from each ROI for each subject on the basis of the specified atlas.

B. Experimental Process and Details

We randomly selected 10% of patient samples from the dataset as input into the ROI spatial structure analysis module. For each subject in the dataset, the fMRI time series was randomly cropped to 128 samples along the temporal dimension to maximize the retention of the sample information. ROI parcellation was determined using two public brain atlases: the Schaefer atlas [44] and the AAL atlas [45]. For the Schaefer atlas, we selected the scale of 400 ROIs across seven intrinsic connectivity networks. The AAL atlas partitions the brain anatomically into 116 ROIs. The STARFormer model was trained for 100 epochs with a batch size of 128 and a dropout rate of 0.5. Eight attention heads were specified, each with 16 dimensions. For training on ABIDE-I dataset, the initial

learning rate was set to $5e-5$, with a maximum of $1e-4$, and gradually reduced to $1e-5$. For training on ADHD-200 dataset, the initial learning rate was set to $1e-5$, with a maximum of $5e-5$, and finally reduced to $1e-6$.

The experiments were conducted by using PyTorch based on an NVIDIA RTX 2080Ti GPU. We evaluated the performance of the proposed model using a 10-fold cross-validation, and divided the data into a non-overlapping training set (80%), a validation set (10%), and a test set (10%). The model was trained using the Adam optimizer, with cross-entropy loss as the loss function. To comprehensively evaluate the performance of the model, we employed four commonly used metrics, including accuracy (Acc), precision (Prec), recall (Rec), and area under curve (AUC).

C. Competing Methods

Advanced traditional baselines (SVM [46], LSTM [27], BrainNetCNN [47]), transformer-based models (SwinTransformer [37], BoIT [28], Com-BrainTF [48]), and graph neural networks (GNN) (MAHGCN [49], RGTNet [50], PLSNet [51]) were selected for comparison with STARFormer. The architectures, loss functions, and learning rate schedulers for each competing method were adopted from their original papers and subsequently fine-tuned in the experimentation to ensure optimal and competitive performance.

V. RESULTS

A. Comparative Studies

We demonstrate the results of STARFormer in brain disorder diagnosis tasks on ABIDE-I and ADHD-200 datasets using different brain atlases. Table I and Table II present the results of using the Schaefer atlas and the AAL atlas, respectively. It is evident from these tables that our proposed model achieves optimal performance in each metric ($p \leq 0.05$, Wilcoxon signed-rank test), except for PLSNet offering higher precision on ADHD-200. As expected, different atlases lead to variations in metrics. Specifically, the results using the Schaefer atlas consistently outperform those using the AAL atlas. This is reasonable, as the brain graph based on the former has almost four times the number of ROIs compared to the latter, providing a more comprehensive and detailed information of the brain. Fig. 3 intuitively shows the comparative performance between different model categories. Each point in the radar plots represents the averaged performance of the methods within the same category, providing an intuitive visualization of the relative strengths of different approaches. The plots clearly demonstrate that STARFormer consistently achieves superior performance across all metrics compared to other baseline methods.

Note that GNN-based methods generally perform better than most models, probably because GNNs have a natural advantage in learning topological information from the brain. Modelling brain functional network as a graph, GNNs can effectively capture connections between brain regions. However, GNN-based methods mainly take static FC as input, which may struggle to capture dynamic information that changes over time. Furthermore, the relative disadvantage of conventional

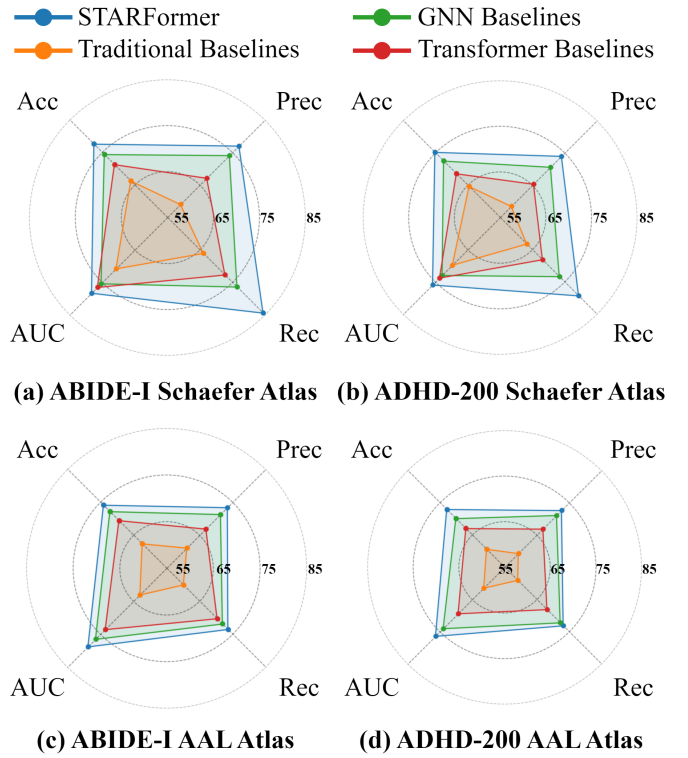


Fig. 3. Radar plots for comparing the performance metrics of different methods on ABIDE-I and ADHD-200 datasets using Schaefer and AAL atlases.

transformer models in fMRI tasks compared to GNN models includes their lack of focus on spatial information. This is because conventional transformers are mainly based on attention mechanisms to capture temporal relationships. In contrast, STARFormer considers the spatial relationships between brain regions while capturing the temporal relationships in the time series. This gives STARFormer a significant performance advantage in brain disorder diagnosis tasks compared to both the transformer baseline models and the GNN baseline models.

B. Ablation Studies

We conducted a series of ablation studies to assess the contributions of the design elements in STARFormer. These design elements include the variable window, cross-window attention, spatio-temporal feature fusion module, and ROI spatial structure analysis module. Starting with a standard transformer variant, we gradually introduced the design elements to create ablation variants. For all ablation variants, the architecture and hyperparameters of the components used were matched to those of STARFormer. The standard variant omits all design elements and retains only the fundamental transformer of the temporal branch with a self-attention mechanism. In order to evaluate the contribution of the variable window, a multi-layer transformer block was introduced, and the time series was divided by variable window. Cross-window attention was introduced to form a new variant to assess its contribution. It is important to note that cross-window attention relies on the variable window, thus self-attention was used when the

TABLE I
PERFORMANCE COMPARISON USING THE SCHAEFER ATLAS ON ABIDE-I AND ADHD-200 DATASETS.

Schaefer	Model	ABIDE-I				ADHD-200			
		Acc	Prec	Rec	AUC	Acc	Prec	Rec	AUC
Traditional	SVM [46]	65.72±4.11	53.97±7.33	66.26±6.68	71.33±4.62	59.76±2.68	59.34±5.32	59.61±5.43	60.62±4.66
	LSTM [27]	66.78±4.25	64.05±9.93	65.81±7.62	70.25±3.85	65.06±3.96	62.92±4.30	60.48±6.38	65.56±5.57
	BrainNetCNN [47]	67.34±4.22	63.82±8.73	65.50±4.63	73.15±5.62	66.78±3.90	62.62±4.66	62.82±8.33	62.22±4.13
Transformer	SwinT [37]	69.79±4.59	60.75±7.60	68.27±6.56	74.13±4.15	68.56±4.74	65.25±4.36	66.40±9.70	73.85±4.59
	BoIT [28]	71.28±4.62	69.85±4.94	71.32±4.35	77.46±3.44	70.82±3.57	68.04±4.18	71.51±3.27	73.36±3.86
	Com-BrainTF [48]	72.75±4.56	70.65±4.54	78.43±4.63	77.93±3.02	68.94±2.68	67.36±4.23	72.92±3.88	73.54±3.68
GNN	MAHGCN [49]	73.12±3.63	71.05±5.38	72.02±4.14	72.07±3.03	70.76±4.63	69.95±3.38	71.08±2.14	74.25±3.41
	RGTNet [50]	74.43±4.82	73.67±4.38	75.28±4.06	74.55±2.73	72.03±3.11	70.14±3.81	71.33±4.45	74.28±2.82
	PLSNet [51]	75.17±4.62	75.91±3.65	79.82±5.83	77.03±2.17	72.53±4.27	73.69±3.82	72.42±3.22	78.02±2.87
Ours	STARFormer	77.57±3.70	76.98±3.27	84.38±3.50	78.29±3.23	74.12±2.47	73.37±3.07	73.54±3.27	78.81±2.18

TABLE II
PERFORMANCE COMPARISON USING THE AAL ATLAS ON ABIDE-I AND ADHD-200 DATASETS.

AAL	Model	ABIDE-I				ADHD-200			
		Acc	Prec	Rec	AUC	Acc	Prec	Rec	AUC
Traditional	SVM [46]	63.74±3.99	52.35±7.18	63.60±6.35	69.90±4.53	57.96±2.60	56.96±5.16	57.82±5.16	59.40±4.52
	LSTM [27]	64.77±4.12	62.12±9.73	63.17±7.24	68.84±3.77	62.10±3.84	60.69±4.17	58.66±6.06	64.24±5.40
	BrainNetCNN [47]	65.31±4.09	60.90±8.56	62.88±4.40	70.68±5.51	61.77±3.78	60.11±4.52	60.63±7.91	60.77±4.01
Transformer	SwinT [37]	65.69±4.45	58.92±7.45	60.53±0.53	72.64±4.07	66.50±4.60	62.64±4.23	65.22±9.22	66.29±4.45
	BoIT [28]	69.41±2.15	68.52±4.07	66.49±4.22	73.30±3.51	67.66±3.46	68.15±4.05	68.36±5.01	69.83±3.74
	Com-BrainTF [48]	70.56±4.42	68.53±4.41	77.21±4.25	75.37±2.96	66.87±2.60	69.74±4.10	70.73±3.59	72.06±3.51
GNN	MAHGCN [49]	71.31±3.52	69.40±3.27	70.09±3.93	71.11±2.97	69.69±2.49	71.36±3.28	70.19±4.23	71.86±3.31
	RGTNet [50]	73.19±3.68	71.45±3.29	73.22±3.86	72.32±2.68	70.06±2.96	70.02±3.65	73.41±3.70	74.75±2.74
	PLSNet [51]	72.97±3.48	70.87±3.54	76.62±3.54	75.46±3.25	70.53±3.14	71.81±2.03	72.97±4.86	75.45±2.78
Ours	STARFormer	75.19±2.93	73.96±2.13	79.27±3.42	75.91±2.85	72.92±2.40	72.59±2.02	73.12±3.23	76.39±2.45

variable window was absent. To evaluate the contribution of spatial features, the spatio-temporal feature fusion module was incorporated into the variants, forming two variants based on the variable window with and without cross-window attention. Finally, the contribution of spatial features together with ROI analysis was evaluated by introducing ROI spatial structure analysis module.

Table III lists the performance metrics of all ablation variants, showing that the STARFormer model, which incorporates all design elements, achieves the highest performance among all variants. First, the inclusion of the variable window

significantly enhances the performance of the transformer, demonstrating that extracting local features at different scales is more practical than directly extracting global representations. Second, we find that using cross-window attention to facilitate information interaction across windows improves performance, indicating the importance of this cross-window attention mechanism for integrating contextual representations of local features across windows. Third, when both temporal and spatial features are extracted and analyzed simultaneously, all performance metrics show improvement. This is because attention to spatial information provides the model with more

TABLE III
ABLATION STUDY OF DIFFERENT COMPONENTS ON ABIDE-I AND ADHD-200 DATASETS.

Variable Window	Cross-Window Attention	Spatial Feature	ROI Analysis	ABIDE-I				ADHD-200			
				Acc	Prec	Rec	AUC	Acc	Prec	Rec	AUC
×	×	×	×	66.82±2.91	66.82±2.16	70.81±4.95	71.67±6.26	65.32±4.31	63.11±4.92	60.43±6.10	65.96±5.51
✓	×	×	×	71.18±2.99	67.62±3.02	75.98±5.35	74.28±3.58	68.06±3.26	68.51±4.07	68.63±4.37	70.83±3.83
✓	✓	×	×	73.36±5.03	70.39±4.57	81.84±5.76	75.74±3.58	68.90±2.65	68.63±3.51	70.52±3.53	71.54±3.49
✓	×	✓	×	74.26±3.93	72.11±4.77	82.33±5.35	76.48±4.57	70.79±2.30	70.16±3.11	71.03±3.97	73.24±3.01
✓	✓	✓	×	75.38±4.36	73.78±5.18	83.13±5.16	76.44±4.92	71.57±2.94	71.64±3.82	71.36±4.04	74.96±3.22
✓	✓	✓	✓(R)	59.18±3.21	63.87±6.67	63.55±7.12	57.71±3.90	58.63±4.32	60.33±5.21	61.24±5.76	59.52±4.00
✓	✓	✓	✓(E)	77.57±3.70	76.98±3.27	84.38±3.50	78.29±3.23	74.12±2.47	73.37±3.07	73.54±3.27	78.81±2.18

Notes: The elements of ablation include the variable window, cross-window attention, spatio-temporal feature fusion module (Spatial Feature), and ROI spatial structure analysis module (ROI Analysis). When the ROI spatial structure analysis module is enabled, (R) denotes the random permutation of the ROI sequence, and (E) indicates the ROI arranged based on EC. The results are based on the Schaefer atlas.

TABLE IV
THE COMPARISON OF PERFORMANCE WITH DIFFERENT VARIABLE WINDOW SETTINGS ON ABIDE-I AND ADHD-200 DATASETS.

Variable Window	ABIDE-I				ADHD-200			
	Acc	Prec	Rec	AUC	Acc	Prec	Rec	AUC
{8, 4, 4, 8}	75.29±4.18	75.64±3.94	82.27±4.01	77.09±3.67	72.91±2.84	68.87±3.54	72.62±3.45	76.63±3.52
{16, 8, 8, 16}	75.86±4.02	75.98±4.40	84.13±3.16	77.51±3.35	73.79±2.75	69.04±3.18	73.51±3.37	78.36±3.68
{8, 4, 2, 2, 4, 8}	76.78±4.36	75.87±3.18	84.41±3.79	77.44±3.92	73.82±3.51	70.45±3.20	74.22±3.86	78.32±2.68
{16, 8, 4, 4, 8, 16}	77.57±3.70	76.98±3.27	84.38±3.50	78.29±3.23	74.12±2.47	73.37±3.07	73.54±3.27	78.81±2.18
{16, 8, 4, 2, 2, 4, 8, 16}	74.77±3.00	72.25±3.32	83.01±3.53	76.96±4.33	72.53±3.11	68.88±3.27	71.57±4.31	76.45±2.97

comprehensive information, thereby having better classification results. Additionally, randomly shuffling the ROI spatial ordering of brain regions leads to a significant drop in model performance due to the disorder among brain regions. Finally, we observe that ranking ROIs within the functional brain network based on EC significantly contributes to improving model performance. We speculate that this is because effective connectivity captures the directional flow of information between different brain regions, and EC distinguishes the ability of nodes to receive and transmit information within the network, making it easier for the model to identify potential features when extracting spatial information. In summary, the use of different ROI spatial ordering for brain regions affects the final results, highlighting the critical importance of spatial information for fMRI data.

C. Window Setting

We evaluated the STARFormer variants obtained from different windows applied to fMRI time series. The Table IV lists the performance metrics of different variants of STARFormer variable windows using the ABIDE-I dataset and the ADHD-

200 dataset based on the Schaefer atlas. We observed that the performance advantage of the variable window maximizes when the number of window tokens is {16, 8, 4, 4, 8, 16}. This may be because too few layers lead to insufficient learning capacity of the model, preventing it from extracting enough features, while too many layers may cause the model to overfit, resulting in good performance on the training set but poor generalization to the test set. Additionally, since the number of window tokens determines the size of the window, smaller window tokens allow the model to focus more on local features, enabling it to capture detailed information better. However, smaller window tokens will limit the ability of the model to perceive global information, making it difficult to understand broader feature dependencies, especially in tasks that require capturing cross-regional or long-term dependencies. In contrast, larger window tokens are capable of capturing global features.

As shown in Fig. 5, we examined the impact of the size of the extended window under a specific setting of variable window on model performance, training with extended window of sizes $w/4$, $w/2$, and w . We found that performance exhibits

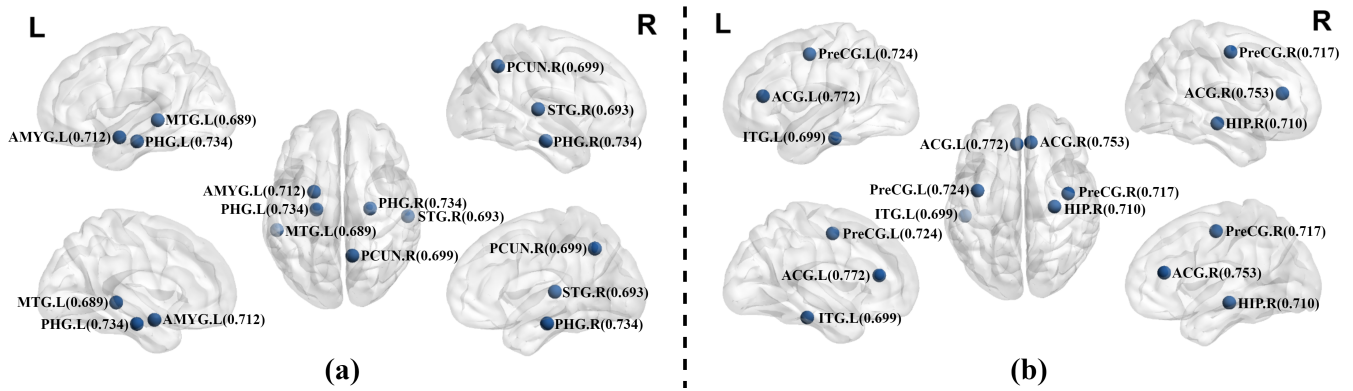


Fig. 4. Top 5% ROIs which are most important for ASD classification (a) and ADHD classification (b) according to importance scores based on the attention matrix in the transformer block of STARFormer.

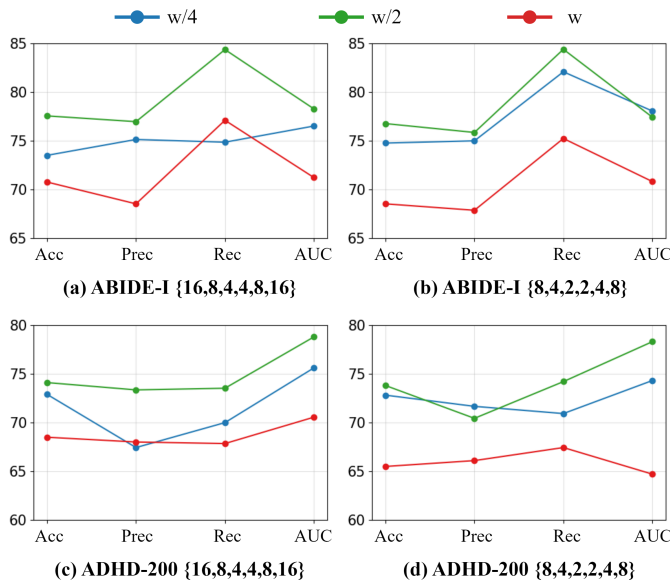


Fig. 5. The comparison of the performance of STARFormer variants with the configurations of different extended window based on ABIDE-I and ADHD-200 datasets.

moderate variation with changes in the extended window token size. In other words, the model tends to achieve optimal performance with a window size of $w/2$. Overall, the size of the window needs to be set with a balance between the needs for local and global information. We found that both datasets typically achieved optimal or near-optimal performance when the number of window tokens for the variable window was $\{16, 8, 4, 4, 8, 16\}$ and the extended window size was $w/2$. This result indicates a degree of reliability in the introduction of window-related design elements in STARFormer.

VI. DISCUSSION

A. Interpretability Analysis

We used interpretability techniques to further analyze brain regions important for ASD and ADHD in the STARFormer model. In the temporal branch, the attention matrices (i.e., the Attention(Q, K, V) defined in Equation (13)) of each layer are averaged. In the spatial branch, the attention matrices

are multiplied by the feature activation values. Subsequently, the results of the temporal and spatial branches are each aggregated by rows and normalized to obtain attention importance scores for temporal and spatial dimensions. Finally, by combining these two scores through weighted summation, a comprehensive importance score is obtained to identify the most influential ROIs.

As shown in Fig. 4, we present the top 5% most influential ROIs for diagnosing ASD and ADHD. A manual review confirmed that all identified ROIs are consistent with the previous literature, linking them with the neural manifestations of ASD and ADHD. For instance, functional abnormalities in the parahippocampal gyrus may impair the ability of individuals with ASD to adapt or recall relevant information in social settings, affecting their social behavior [18]. Similarly, functional abnormalities in the amygdala can lead to anxiety or avoidance in social situations for those with ASD [52]. In addition, functional abnormalities in the precentral gyrus have been associated with hyperactivity symptoms in individuals with ADHD [53], while abnormalities in the inferior temporal gyrus can result in attention deficits or distractibility during complex visual tasks [54]. Overall, this demonstrates that the STARFormer effectively captures brain activation patterns in both healthy individuals and those with brain disorders.

B. Limitation and Future Work

While our proposed STARFormer shows significant improvement over existing computer-aided diagnosis methods for brain disorders, several issues should be considered in future work. First, we used node centrality measures to extract spatial information for ROIs rather than directly using the topological information of the brain network. Future research could explore using graph encoding to model brain topology. Second, auxiliary information about patients, such as personal details or scanning protocols, was not included as input to the model. Recent studies suggest that these phenotypic data complement imaging data and may improve the diagnosis of brain disorders [55]. Therefore, it is reasonable to expect that integrating phenotypic information could further improve the classification performance of STARFormer. Lastly, considering the challenges in data acquisition in clinical settings, many

subjects will have partially labeled fMRI data. Thus, strategies using semi-supervised or unsupervised learning could be considered for training.

VII. CONCLUSION

In this study, we introduce STARFormer, an advanced transformer-based framework for diagnosing brain disorders that effectively integrates spatial structure analysis with temporal feature learning. Through its novel architecture, STARFormer successfully addresses key limitations of existing methods by simultaneously capturing the intricate spatial relationships between brain regions and both local and global temporal patterns in fMRI data.

Comprehensive empirical evaluations of the ABIDE-I and ADHD-200 datasets demonstrate that STARFormer achieves superior performance in both ASD and ADHD classification tasks, significantly outperforming existing state-of-the-art methods. The framework's ability to identify specific ROIs related to brain disorders aligns with established neurological findings, validating its potential for clinical applications. These results show that STARFormer advances the technical frontier of brain disorder diagnosis. Future research may explore the adaptability of the framework to other neurological disorders and its potential integration into clinical decision support systems.

REFERENCES

- [1] C. Zhang, Y. Ma, L. Qiao, L. Zhang, and M. Liu, "Learning functional brain networks with heterogeneous connectivities for brain disease identification," *Neural Networks*, vol. 180, p. 106660, 2024.
- [2] L. K. Bicks and D. Geschwind, "Functional neurogenomics in autism spectrum disorders: A decade of progress," *Current Opinion in Neurobiology*, vol. 86, p. 102858, 2024.
- [3] S. Koirala et al., "Neurobiology of attention-deficit hyperactivity disorder: historical challenges and emerging frontiers," *Nature Reviews Neuroscience*, vol. 25, p. 759–775, 2024.
- [4] M. Pievani et al., "Functional network disruption in the degenerative dementias," *The Lancet Neurology*, vol. 10, no. 9, pp. 829–843, 2011.
- [5] C. Y. Wee et al., "Disrupted brain functional network in internet addiction disorder: a resting-state functional magnetic resonance imaging study," *PLoS One*, vol. 9, no. 9, p. e107306, 2014.
- [6] X. Qian et al., "Large-scale brain functional network topology disruptions underlie symptom heterogeneity in children with attention-deficit/hyperactivity disorder," *NeuroImage: Clinical*, vol. 21, p. 101600, 2019.
- [7] "Disentangle the group and individual components of functional connectome with autoencoders," *Neural Networks*, vol. 181, p. 106786, 2025.
- [8] Y. Li et al., "MHNet: Multi-view high-order network for diagnosing neurodevelopmental disorders using resting-state fMRI," *arXiv preprint arXiv:2407.03217*, 2024.
- [9] "Fusing multi-scale functional connectivity patterns via multi-branch vision transformer (MB-ViT) for macaque brain age prediction," *Neural Networks*, vol. 179, p. 106592, 2024.
- [10] M. Khosla et al., "Machine learning in resting-state fMRI analysis," *Magnetic Resonance Imaging*, vol. 64, pp. 101–121, 2019.
- [11] A. Shoeibi et al., "Diagnosis of brain diseases in fusion of neuroimaging modalities using deep learning: A review," *Information Fusion*, vol. 93, pp. 85–117, 2023.
- [12] A. Vaswani, "Attention is all you need," *Advances in Neural Information Processing Systems*, vol. 30, 2017.
- [13] S. Cong et al., "Comprehensive review of transformer-based models in neuroscience, neurology, and psychiatry," *Brain-X*, vol. 2, no. 2, p. e57, 2024.
- [14] V. Mubonanyikuzo et al., "Detection of Alzheimer's Disease in neuroimages using Vision Transformers: A systematic review and meta-analysis (preprint)," *Journal of Medical Internet Research*, 2024.
- [15] R. M. Hutchison et al., "Dynamic functional connectivity: promise, issues, and interpretations," *Neuroimage*, vol. 80, pp. 360–378, 2013.
- [16] M. P. van den Heuvel and O. Sporns, "A cross-disorder connectome landscape of brain dysconnectivity," *Nature Reviews Neuroscience*, vol. 20, no. 7, pp. 435–446, 2019.
- [17] L. J. Zheng et al., "Altered amygdala and hippocampus effective connectivity in mild cognitive impairment patients with depression: a resting-state functional mr imaging study with granger causality analysis," *Oncotarget*, vol. 8, no. 15, p. 25021, 2017.
- [18] C. S. Monk et al., "Abnormalities of intrinsic functional connectivity in autism spectrum disorders," *Neuroimage*, vol. 47, no. 2, pp. 764–772, 2009.
- [19] P. Saha, "Eigenvector centrality characterization on fMRI data: Gender and node differences in normal and ASD subjects," *Journal of Autism and Developmental Disorders*, vol. 54, no. 7, pp. 2757–2768, 2024.
- [20] B. T. Grobely et al., "Betweenness centrality of intracranial electroencephalography networks and surgical epilepsy outcome," *Clinical Neurophysiology*, vol. 129, no. 9, pp. 1804–1812, 2018.
- [21] H. Liao et al., "Changes in degree centrality of network nodes in different frequency bands in Parkinson's disease with depression and without depression," *Frontiers in Neuroscience*, vol. 15, p. 638554, 2021.
- [22] J. Zhou et al., "LCGNet: Local sequential feature coupling global representation learning for functional connectivity network analysis with fMRI," *IEEE Transactions on Medical Imaging*, vol. 43, no. 12, pp. 4319–4330, 2024.
- [23] Y. Wang et al., "A deep dynamic causal learning model to study changes in dynamic effective connectivity during brain development," *IEEE Transactions on Biomedical Engineering*, vol. 71, no. 12, pp. 3390–3401, 2024.
- [24] P. Dai et al., "Altered effective connectivity among the cerebellum and cerebrum in patients with major depressive disorder using multisite resting-state fMRI," *The Cerebellum*, vol. 22, no. 5, pp. 781–789, 2023.
- [25] M. G. Sharaev et al., "Effective connectivity within the default mode network: dynamic causal modeling of resting-state fMRI data," *Frontiers in Human Neuroscience*, vol. 10, p. 14, 2016.
- [26] X. Deng et al., "Classifying ASD based on time-series fMRI using spatial-temporal transformer," *Computers in Biology and Medicine*, vol. 151, p. 106320, 2022.
- [27] N. C. Dvornek et al., "Identifying autism from resting-state fMRI using long short-term memory networks," in *Machine Learning in Medical Imaging: 8th International Workshop, MLMI 2017, Held in Conjunction with MICCAI 2017, Quebec City, QC, Canada, September 10, 2017, Proceedings 8*, pp. 362–370, Springer, 2017.
- [28] H. A. Bedel et al., "BoIT: Fused window transformers for fMRI time series analysis," *Medical Image Analysis*, vol. 88, p. 102841, 2023.
- [29] G. Wang et al., "Multi modality fusion transformer with spatio-temporal feature aggregation module for psychiatric disorder diagnosis," *Computerized Medical Imaging and Graphics*, vol. 114, p. 102368, 2024.
- [30] X. Li et al., "2-channel convolutional 3D deep neural network (2CC3D) for fMRI analysis: ASD classification and feature learning," in *2018 IEEE 15th International Symposium on Biomedical Imaging (ISBI 2018)*, pp. 1252–1255, IEEE, 2018.
- [31] L. Zou et al., "3D CNN based automatic diagnosis of attention deficit hyperactivity disorder using functional and structural MRI," *Ieee Access*, vol. 5, pp. 23626–23636, 2017.
- [32] R. Liu et al., "Spatial-temporal co-attention learning for diagnosis of mental disorders from resting-state fMRI data," *IEEE Transactions on Neural Networks and Learning Systems*, vol. 35, no. 8, pp. 10591–10605, 2023.
- [33] W. Zhang et al., "STANet: A novel spatio-temporal aggregation network for depression classification with small and unbalanced FMRI data," *Tomography*, vol. 10, no. 12, pp. 1895–1914, 2024.
- [34] P. He et al., "A spatiotemporal graph transformer approach for Alzheimer's disease diagnosis with rs-fMRI," *Computers in Biology and Medicine*, vol. 178, p. 108762, 2024.
- [35] A. Shojaie and E. B. Fox, "Granger causality: A review and recent advances," *Annual Review of Statistics and Its Application*, vol. 9, no. 1, pp. 289–319, 2022.
- [36] B. T. Yeo et al., "The organization of the human cerebral cortex estimated by intrinsic functional connectivity," *Journal of neurophysiology*, vol. 106, no. 3, pp. 1125–1165, 2011.
- [37] Z. Liu et al., "Swin transformer: Hierarchical vision transformer using shifted windows," in *Proceedings of the IEEE/CVF International Conference on Computer Vision*, pp. 10012–10022, 2021.
- [38] J. Yang et al., "Focal self-attention for local-global interactions in vision transformers," *arXiv preprint arXiv:2107.00641*, 2021.

- [39] D. Hendrycks and K. Gimpel, "Gaussian error linear units (GELUS)," *arXiv preprint arXiv:1606.08415*, 2016.
- [40] C. Craddock et al., "The neuro bureau preprocessing initiative: open sharing of preprocessed neuroimaging data and derivatives," *Frontiers in Neuroinformatics*, vol. 7, no. 27, p. 5, 2013.
- [41] P. Bellec et al., "The neuro bureau ADHD-200 preprocessed repository," *Neuroimage*, vol. 144, pp. 275–286, 2017.
- [42] C. Craddock et al., "Towards automated analysis of connectomes: The configurable pipeline for the analysis of connectomes (C-PAC)," *Front Neuroinform*, vol. 7, 2013.
- [43] P. Bellec et al., "The neuro bureau ADHD-200 preprocessed repository," *Neuroimage*, vol. 144, pp. 275–286, 2017.
- [44] A. Schaefer et al., "Local-global parcellation of the human cerebral cortex from intrinsic functional connectivity MRI," *Cerebral Cortex*, vol. 28, no. 9, pp. 3095–3114, 2018.
- [45] N. Tzourio-Mazoyer et al., "Automated anatomical labeling of activations in SPM using a macroscopic anatomical parcellation of the MNI MRI single-subject brain," *Neuroimage*, vol. 15, no. 1, pp. 273–289, 2002.
- [46] A. Abraham et al., "Deriving reproducible biomarkers from multi-site resting-state data: An Autism-based example," *NeuroImage*, vol. 147, pp. 736–745, 2017.
- [47] J. Kawahara et al., "BrainNetCNN: Convolutional neural networks for brain networks; towards predicting neurodevelopment," *NeuroImage*, vol. 146, pp. 1038–1049, 2017.
- [48] A. Bannabdhavi et al., "Community-aware transformer for autism prediction in fmri connectome," in *International Conference on Medical Image Computing and Computer-Assisted Intervention*, pp. 287–297, Springer, 2023.
- [49] M. Liu et al., "Hierarchical graph convolutional network built by multi-scale atlases for brain disorder diagnosis using functional connectivity," *IEEE Transactions on Neural Networks and Learning Systems*, vol. 35, no. 11, pp. 15182–15194, 2023.
- [50] Y. Wang et al., "Residual graph transformer for autism spectrum disorder prediction," *Computer Methods and Programs in Biomedicine*, vol. 247, p. 108065, 2024.
- [51] Y. Wang et al., "PlsNet: Position-aware GCN-based autism spectrum disorder diagnosis via fc learning and rois sifting," *Computers in Biology and Medicine*, vol. 163, p. 107184, 2023.
- [52] N. M. Kleinmans et al., "Reduced neural habituation in the amygdala and social impairments in autism spectrum disorders," *American Journal of Psychiatry*, vol. 166, no. 4, pp. 467–475, 2009.
- [53] D. Lei et al., "Functional MRI reveals different response inhibition between adults and children with ADHD.," *Neuropsychology*, vol. 29, no. 6, p. 874, 2015.
- [54] M. Kobel et al., "Structural and functional imaging approaches in attention deficit/hyperactivity disorder: does the temporal lobe play a key role?," *Psychiatry Research: Neuroimaging*, vol. 183, no. 3, pp. 230–236, 2010.
- [55] J. Zhang, Q. Wang, X. Wang, L. Qiao, and M. Liu, "Preserving specificity in federated graph learning for fMRI-based neurological disorder identification," *Neural Networks*, vol. 169, pp. 584–596, 2024.